Edinburgh Research Explorer

Dynamic Density Functional Theory for Sedimentation Processes on Complex Domains: Modelling, Spectral Elements, and Control Problems

Dynamic Density Functional Theory for Sedimentation Processes on Complex Domains: Modelling, Spectral Elements, and Control Problems

Jonna C. Roden, Benjamin D. Goddard, and John W. Pearson

School of Mathematics and Maxwell Institute for Mathematical Sciences, The University of Edinburgh, Edinburgh, EH9 3FD, UK

(*b.goddard@ed.ac.uk)

Modelling of many real-world processes, such as drug delivery, wastewater treatment, and pharmaceutical production, requires accurate descriptions of the dynamics of hard particles confined in complicated domains. In particular, when modelling sedimentation processes or systems with driven flows, it is important to accurately capture volume exclusion effects. This work applies Dynamic Density Functional Theory to the evolution of a particle density under diffusion, external forces, particle–particle interaction, and volume exclusion. Using a spectral element framework, for the first time it is possible to include all of these effects in dynamic simulations on complex domains. Moreover, this allows one to apply complicated no-flux, and other non-local, non-linear, boundary conditions. The methodology is also extended to control problems, addressing questions of how to enhance production set-up in industrially-motivated processes. In this work the relevant models are introduced, numerical methods are discussed, and several example problems are solved to demonstrate the methods' versatility. It is shown that incorporating volume exclusion is crucial for simulation accuracy and we illustrate that the choice of boundary conditions significantly impacts the dynamics.

I. INTRODUCTION

Many physical processes can be modelled by systems of interacting particles, both in equilibrium and in motion. The particles in such systems can be soft, i.e., they are able to overlap and deform, or hard, in which case they exclude volume. Granular media, colloidal fluids, and liquid crystals can be described by particle system models[33], and even pedestrians, cars, and animals can be modelled as interacting particles[27], for which volume exclusion is a crucial aspect of their dynamics. A common approach is to model volume-excluding particles as approximately spherical with a hard core[33]. Extensions to systems of non-spherical or orientable particles exist, with applications for self-propelled or magnetic particles[56].

The fact that such particles can only occupy a given volume directly impacts on many real-world dynamical situations, such as sedimentation, jamming in flows through constrictions, and the formation of particle clusters. For example, when modelling sedimentation processes without volume exclusion, i.e., as soft particle dynamics, one would find that a very thin layer of overlapping particles is formed at the bottom of the domain. This is not physically accurate for hard particle fluids and describing such processes with a soft particle model would overestimate the density in this region; accurate models of volume exclusion are required in this, and many other, applications.

There are a multitude of different ways of modelling particle dynamics. If one were interested in the dynamics of each individual particle, the size of the system would be limited by computational capacity to systems of around 10^3–10^6 particles. Typical molecular systems, such as water, contain 10^{25} particles per cubic litre. This prohibits the computation of the dynamics of each individual particle, so other approaches have to be employed. For systems in equilibrium, statistical mechanics[34,51] provides a valuable alternative by considering the particle ensemble, and therefore a particle density.

From this formulation (equilibrium) Density Functional Theory (DFT) arose[18,26]. In this theory, the Helmholz free energy, denoted by $\mathscr{F}$, of a system in equilibrium can be expressed as a functional of the one-body particle density, which depends on the three spatial dimensions only and, crucially, not on the number of particles. Following this, the dynamics of such particle systems can be modelled using Dynamic Density Functional Theory (DDFT)[56], which is the dynamic extension of DFT. The key idea in DDFT is that a one-body particle density, denoted by ρ, evolves in space and time according to the Helmholtz free energy of the system. In particular, for non-driven systems (where there is no advective flow and all potentials are time-independent), ρ will evolve towards the equilibrium density ρ_∞, for which $\mathscr{F}$ is minimized. Such DDFT models are complicated integro-partial differential equations (integro-PDEs) that have to be solved numerically, and different numerical methods are available to do so on simple one-, two-, and three-dimensional domains[12,16,21,49]. As above, a key advantage of DFT and DDFT models is that they are independent of the number of particles, and their computation cost (formally) only depends on the dimensions of the spatial domain, while retaining information on the particle scale through the microscopic nature of the free energy (which can capture effects, such as layering of hard spheres, on the scale of the particles themselves).

DDFT is typically applied on simple, e.g., rectangular periodic, domains. However, many real-world dynamics, such as drug delivery[38], sedimentation in industrial processes[23,62], or even crowd dynamics[28], take place on much more complicated domains. It is therefore important to understand how to solve models that include volume exclusion effects on domains that are relevant in real-world applications. Moreover, in applications such as drug delivery or industrial manufacturing processes, it is often crucial to optimize a given process for a desired outcome. For example, one may want to answer the question of how the sedimentation process in an industrial context, such as in brewing[62], wastewater treatment[23], or

Accepted to J. Chem. Phys. 10.1063/5.0166458

DDFT for Sedimentation Processes
2

centrifugation in the pharmaceutical industry[30], can be optimized by varying given parameters in an experimental set up. Such questions can be answered using techniques from optimal control theory. It is clear that if one would like to optimize a process involving hard particles, it is important to incorporate volume exclusion effects into the set-up.

Recently, advances have been made in solving DDFT models for soft particles on complicated domains[41], as well as in solving associated control problems[2,41]. However, until now, these methods had not been applied to more complicated DDFTs, such as those that model volume exclusion. This paper demonstrates how the framework developed in [2] and [41] can be extended to these more complicated DDFT models, which lays a crucial foundation for computing even more sophisticated DDFTs on complex domains, as well as solving control problems involving such models.

The paper is structured as follows: In Section II the equilibrium and dynamic DFT models are introduced, as well as an associated optimal control problem. In Section III the necessary numerical methods are introduced, before some example problems are solved in Section IV. Section V provides some concluding remarks.

II. MODEL EQUATIONS

In this section the relevant models are introduced. First, the equilibrium DFT is discussed to provide the necessary context on modelling volume exclusion. Then the DDFT model that is solved in the present work is introduced. Finally, we discuss an optimal control problem that involves the considered DDFT model, and present (first-order) optimality conditions for solving such a problem.

A. The DFT Model

Equilibrium Density Functional Theory dictates that the Helmholtz free energy, denoted by $\mathscr{F}$, of an open thermodynamic system in equilibrium can be fully determined by a single variable: the one-body particle density ρ. This equilibrium density is found by minimizing $\mathscr{F}$. Foundational references for this theory are [18] and [26]. The general form of $\mathscr{F}$ is given by

$$\mathscr{F}[\rho] = \mathscr{F}_{\text{id}}[\rho] + \mathscr{F}_{\text{ext}}[\rho] + \mathscr{F}_{\text{exc}}[\rho], \quad (1)$$

where the ideal gas and external contributions are known to be

$$\mathscr{F}_{\text{id}}[\rho] = \int_\Omega \rho\,(\ln\rho - 1)\,d\vec{x}, \quad \mathscr{F}_{\text{ext}}[\rho] = \int_\Omega \rho V_{\text{ext}} d\vec{x},$$

respectively, with V_{ext} a given external potential and Ω a given spatial domain. Here, and in the following, we have (without loss of generality) set the de Broglie wavelength and temperature to be equal to one (see, e.g., [56, Eq. (11)] for a version including these parameters). The excess free energy $\mathscr{F}_{\text{exc}}$ is generally not known and subject to approximation, apart from the case of hard rods in one dimension[35].

One widely used and straightforward approximation to the excess free energy is the mean-field approximation, which is given by

$$\mathscr{F}_{\text{MF}}[\rho] = \frac{1}{2}\int_\Omega \int_\Omega \rho(\vec{x})\rho(\vec{x}')V_2(|\vec{x} - \vec{x}'|)d\vec{x}'d\vec{x}, \quad (2)$$

where V_2 is a given two-body interaction potential[37]. This version of $\mathscr{F}_{\text{exc}}$ models soft particles and cannot capture volume exclusion effects, i.e., non-overlapping particles. Such a model can be accurate in low density regimes, but fails to correctly reproduce the dynamics for denser systems.

A successful approach for modelling the excess free energy of hard particle systems is called Fundamental Measure Theory (FMT)[44]. However, this is computationally expensive, since multiple convolution integrals have to be computed over regions determined by the surface and volumes of the particles. The derivation of optimal control problems involving such models and their solution on complicated domains is also highly non-trivial. Instead, in the present work, following [5], we consider a simplification of the FMT approach to model these volume exclusion effects, and leave more complicated models for future work. Following the formulation by Rosenfeld[44], a general excess free energy of a system can be approximated by

$$\mathscr{F}_{\text{exc}}[\rho] = \int_\Omega \Phi[\rho]d\vec{x}, \quad (3)$$

where Φ is the reduced free energy density. For more detail on this, and FMT in general, we refer the reader to the review [46]. Based on the FMT theory for three-dimensional spheres, in which Φ is a complicated expression based on the fundamental measures of a sphere, and on the known exact solution for hard rods in one dimension[35], Rosenfeld derived a version of the FMT theory for two-dimensional hard disks[45]. However, some additional approximations have to be made when choosing the weighted densities (typically convolutions of the density, ρ, with 'fundamental measures' of a sphere, such as its volume or surface area), which is not necessary in one and three dimensions, and there exist alternative formulations[48]. In the uniform limit, for one particle species, the free energy for the bulk fluid is the same as derived by scaled particle theory (SPT)[29,39,40], which also coincides with the Percus–Yevick compressibility equation[36], as detailed in [43]. The result is that

$$\Phi[\rho] = -\rho\ln(1 - a\rho) + \frac{a\rho^2}{1 - a\rho}. \quad (4)$$

Here $\eta := a\rho$, with $a = \pi\sigma^2/4$, is the local packing fraction, depending on the particle diameter σ and the density ρ. While the SPT approximation (4) and its three-dimensional equivalent are used in classical DFT[22,32,47,50,57,63], and other statistical mechanics approaches[13,14,17,24], in DDFT it is not commonly applied and only the work of Archer et al.[4,5,31,64] is known to us in this context.

Combining (3) and (4), the approximation to $\mathscr{F}_{\text{exc}}$ of interest is

$$\mathscr{F}_{\text{VE}}[\rho] = \int_\Omega \left(-\rho\ln(1 - a\rho) + \frac{a\rho^2}{1 - a\rho}\right)d\vec{x}. \quad (5)$$

Note that we require $\rho < 1/a$, since the local packing fraction $\eta < 1$ everywhere in the domain by definition of the model. The approximations $\mathscr{F}_{\mathrm{MF}}$ and $\mathscr{F}_{\mathrm{VE}}$ for the free energy can be combined to model both volume exclusion and attractive or repulsive soft interactions, which has been done in [5]. Then the Helmholtz free energy functional becomes

$$\mathscr{F}[\rho] = \mathscr{F}_{\mathrm{id}}[\rho] + \mathscr{F}_{\mathrm{ext}}[\rho] + \mathscr{F}_{\mathrm{MF}}[\rho] + \mathscr{F}_{\mathrm{VE}}[\rho]. \qquad (6)$$

B. The DDFT Model

Dynamic Density Functional Theory is based on the DFT description of the free energy in terms of the one-body density ρ. DDFT describes the evolution of ρ towards equilibrium, given the free energy $\mathscr{F}$ defined in (1). A comprehensive review of DDFT can be found in [56]. The general form of the model is given by

$$\frac{\partial \rho}{\partial t} = \nabla \cdot \left(\rho \nabla \frac{\delta \mathscr{F}[\rho]}{\delta \rho} \right) \qquad \text{in } (0,T) \times \Omega,$$

$$0 = \rho \nabla \frac{\delta \mathscr{F}[\rho]}{\delta \rho} \cdot \vec{n} \qquad \text{on } (0,T) \times \partial\Omega,$$

$$\rho(0,\vec{x}) = \rho_0(\vec{x}) \qquad \text{on } \{t=0\} \times \Omega,$$

where Ω is the considered domain with boundary $\partial\Omega$, $\vec{n}$ is the outward unit normal, and the time is defined up to some given time horizon T. Note that the boundary conditions chosen here are no-flux conditions and, in particular, are non-local due to the form of $\mathscr{F}_{\mathrm{MF}}$ in (2); its functional derivative corresponds to a convolution between V_2 and ρ. In the present work we almost exclusively consider no-flux boundary conditions, since these are most realistic in many real-world applications, and one of the most complicated cases to treat. One can swap these for Dirichlet, Robin, or periodic conditions straightforwardly in the discussed numerical framework. In one numerical example in Section IV we will compare the results of a model with no-flux boundary conditions against one with periodic boundary conditions.

In order to derive the dynamic model explicitly in terms of the free energy given in (6), we need to take the appropriate derivatives of the term that captures volume exclusion, given by (5). We obtain

$$j_{\mathrm{VE}}(\rho) := -\rho \nabla \frac{\delta \mathscr{F}_{\mathrm{VE}}[\rho]}{\delta \rho} = -\frac{a\rho \nabla \rho}{1-a\rho} + \rho \nabla \frac{a\rho - 2}{(a\rho - 1)^2}. \quad (7)$$

Equivalent standard calculations for the other terms in (6) result in an extended mean-field DDFT model, see e.g., [56], for the mean-field model without the additional term. This results

in

$$\frac{\partial \rho}{\partial t} = \nabla^2 \rho - \nabla \cdot j_{\mathrm{VE}}(\rho) + \nabla \cdot (\rho \nabla V_{\mathrm{ext}}) \qquad (8)$$

$$+ \nabla \cdot \int_\Omega \rho(t,\vec{x})\rho(t,\vec{x}')\nabla V_2(|\vec{x}-\vec{x}'|)d\vec{x}' \quad \text{in } (0,T) \times \Omega,$$

$$0 = \frac{\partial \rho}{\partial n} - j_{\mathrm{VE}}(\rho) \cdot \vec{n} + \rho \frac{\partial V_{\mathrm{ext}}}{\partial n}$$

$$+ \int_\Omega \rho(t,\vec{x})\rho(t,\vec{x}')\frac{\partial V_2(|\vec{x}-\vec{x}'|)}{\partial n}d\vec{x}' \quad \text{on } (0,T) \times \partial\Omega,$$

$$\rho(0,\vec{x}) = \rho_0(\vec{x}) \qquad \qquad \text{on } \{t=0\} \times \Omega.$$

This DDFT model captures approximate volume exclusion effects in the particle dynamics. Removing the term j_{VE} recovers the mean-field DDFT model. It can be solved on complicated domains using the MultiShape package, as described in [41]. The numerical methods used to solve (8) are briefly discussed in Section III and numerical examples are presented in Section IV.

C. The Control Problem

In addition to solving the forward DDFT model, a problem of considerable interest is that of optimizing particle distributions arising from such processes. Therefore, we now consider applying the DDFT model as a PDE constraint within a control problem. We refer to [61] for a general discussion of optimal control problems with PDE constraints, and to [2, 3, 41] for optimal control with mean-field DDFT models as constraints. We note that the mathematical analysis of such non-linear problems is highly challenging; see, e.g., [11]. In this section, we will outline the necessary aspects of the optimal control framework for the DDFT model (8).

The control problem of interest is

$$\min_{\rho,\vec{w}} \left[\mathscr{J}(\rho,\vec{w}) := \frac{1}{2}\|\rho - \widehat{\rho}\|^2_{L^2((0,T)\times\Omega)} + \frac{\gamma}{2}\|\vec{w}\|^2_{L^2((0,T)\times\Omega)} \right]$$
$$(9)$$

subject to

$$\frac{\partial \rho}{\partial t} = -\nabla \cdot (\mathscr{D}(\rho) + j_{\mathrm{VE}}(\rho) + \mathscr{I}(\rho) + \rho\vec{w}) \quad \text{in } (0,T) \times \Omega,$$

$$0 = (\mathscr{D}(\rho) + j_{\mathrm{VE}}(\rho) + \mathscr{I}(\rho) + \rho\vec{w}) \cdot \vec{n} \quad \text{on } (0,T) \times \partial\Omega,$$

$$\rho(0,\vec{x}) = \rho_0(\vec{x}) \qquad \qquad \text{on } \{t=0\} \times \Omega,$$

with j_{VE} given by (7),

$$\mathscr{D}(\rho) = -\nabla \rho - \rho \nabla V_{\mathrm{ext}},$$

$$\mathscr{I}(\rho) = -\int_\Omega \rho(t,\vec{x})\rho(t,\vec{x}')\nabla V_2(|\vec{x}-\vec{x}'|)d\vec{x}',$$

γ a given *regularization parameter*, and $\widehat{\rho}$ a given *desired density* that may depend on both time and space. Note that in comparison to DDFT model (8), the PDE constraint in (9) contains the additional term involving $\vec{w}$, which is an advective field. It can be viewed as a generalization of the conservative external force contribution ∇V_{ext}.

Accepted to J. Chem. Phys. 10.1063/5.0166458

DDFT for Sedimentation Processes   4

The aim of solving this problem is to minimize the cost functional $\mathscr{J}$, which is achieved by driving the particle density ρ towards the desired density $\widehat{\rho}$, as measured in the given norm. This is the role of the control variable, denoted by $\vec{w}$, which in this problem is the advective field, and drives the DDFT model towards the desired state. The use of control is penalized in the second term in the cost functional $\mathscr{J}$. How much control is permitted to be invested is dependent on the regularization parameter γ. If γ is small, the control is permitted to be large, and ρ is more likely to be close to $\widehat{\rho}$. If γ is large, less control may be applied to the system and one may not approach $\widehat{\rho}$ as closely. In general, the value of γ is a modelling choice. When designing and testing optimization algorithms one is primarily interested in the robustness of the method for a range of γ values.

Note that one can, as above, and discussed in [2], swap the flow control term for a source control term and no-flux boundary conditions for Dirichlet, Robin, or periodic boundary conditions without much additional work. The choice of boundary conditions in the present work is motivated by the applications of interest.

1. First-Order Optimality System

In order to solve the control problem outlined above, one has to derive and solve the so-called first-order (necessary) optimality system. This system is derived using a Lagrangian approach. The general approach can be found in [61], while a discussion of the derivation of the present system without the volume exclusion term j_{VE} can be found in [2]. Here, we briefly state the Lagrangian formulation and the resulting optimality system.

We highlight at this stage that the focus of this section is not on theoretical questions such as existence and uniqueness of solutions for the problem (9), which are interesting and important questions in their own right, and are highly challenging for problems with quasi-linear PDE constraints. Indeed, for non-linear problems of this form, it is possible for numerical methods to arrive at local minima, even if a global minimum exists. What is of interest here is a proof-of-concept as to whether the numerical methods of this paper can generate a control variable which reduces the cost functional $\mathscr{J}(\rho, \vec{w})$ as opposed to a setting of applying no control, and simulate realistic particle dynamics. As such, we wish to show that the technologies presented in this paper may be applied to that end.

Proceeding formally, the Lagrangian for the system (9) is defined as

$$\mathscr{L}(\rho, \vec{w}, q, q_{\partial\Omega}) = \mathscr{J}(\rho, \vec{w})$$
$$- \int_0^T \int_\Omega \left(\frac{\partial \rho}{\partial t} + \nabla \cdot (\mathscr{D}(\rho) + j_{VE}(\rho) + \mathscr{I}(\rho) + \rho\vec{w}) \right) q \, d\vec{x}dt$$
$$- \int_0^T \int_{\partial\Omega} (\mathscr{D}(\rho) + j_{VE}(\rho) + \mathscr{I}(\rho) + \rho\vec{w}) \cdot \vec{n} \, q_{\partial\Omega} \, d\vec{x}dt.$$

Note the introduction of the Lagrange multipliers for imposing the PDE system, with q enforcing the PDE constraint and

$q_{\partial\Omega}$ the boundary condition. In order to derive the first-order optimality system, one has to examine

$$\mathscr{L}_q(\rho, \vec{w}, q, q_{\partial\Omega})h = 0, \quad \mathscr{L}_{q_{\partial\Omega}}(\rho, \vec{w}, q, q_{\partial\Omega})h = 0,$$
$$\mathscr{L}_\rho(\rho, \vec{w}, q, q_{\partial\Omega})h = 0, \quad \mathscr{L}_{\vec{w}}(\rho, \vec{w}, q, q_{\partial\Omega})\vec{h} = \vec{0}.$$

Computing $\mathscr{L}_q(\rho, \vec{w}, q, q_{\partial\Omega})h = 0$ and $\mathscr{L}_{q_{\partial\Omega}}(\rho, \vec{w}, q, q_{\partial\Omega})h = 0$, one recovers the DDFT model (8) with corresponding boundary conditions.

Computing $\mathscr{L}_\rho(\rho, \vec{w}, q, q_{\partial\Omega})h = 0$ results in the following adjoint equation:

$$\frac{\partial q}{\partial t} = \mathscr{D}^*(q) + j_{VE}^*(q, \rho) + \mathscr{I}^*(q, \rho) - \vec{w} \cdot \nabla q - \rho + \widehat{\rho}$$
$$\text{in } (0, T) \times \Omega, \quad (10)$$
$$0 = -\frac{1 + a\rho}{(a\rho - 1)^3} \nabla q \cdot \vec{n} \qquad \text{on } (0, T) \times \partial\Omega,$$
$$q(T, \vec{x}) = 0 \qquad \text{on } \{t = T\} \times \Omega,$$

where the boundary condition can in principle be simplified to a Neumann condition. The operators are defined as

$$\mathscr{D}^*(q) := -\nabla^2 q + \nabla V_{\text{ext}} \cdot \nabla q,$$
$$\mathscr{I}^*(q, \rho) := \int_\Omega \rho(t, \vec{x}') \left(\nabla_{\vec{x}} q(t, \vec{x}) - \nabla_{\vec{x}'} q(t, \vec{x}') \right)$$
$$\cdot \nabla V_2(|\vec{x} - \vec{x}'|) d\vec{x}',$$

and the form of $\mathscr{I}^*$ results from an assumption of symmetry of V_2. Note that during the derivation an explicit relationship between the Lagrange multipliers q and $q_{\partial\Omega}$ is found, so that $q_{\partial\Omega}$ is eliminated from the system. The variable q is called the adjoint variable. Moreover,

$$j_{VE}^*(q, \rho) := -A(\rho)\nabla^2 q,$$

with

$$A(\rho) := \frac{a\rho}{1 - a\rho} - \frac{a\rho(3 - a\rho)}{(a\rho - 1)^3}.$$

Finally, computing the Fréchet derivative with respect to $\vec{w}$, that is $\mathscr{L}_{\vec{w}}(\rho, \vec{w}, q, q_{\partial\Omega})\vec{h}$, we obtain the descent direction $\gamma\vec{w} + \rho\nabla q$. The first-order optimality system, given by the PDE constraint in (9), adjoint equation (10), and gradient equation based on the descent direction (i.e., $\vec{w} = -\frac{1}{\gamma}\rho\nabla q$), can be solved with the Newton–Krylov algorithm[2,25], in combination with the MultiShape package[41], which are both briefly outlined in Section III. It is also possible to construct iterative updates to the control variable by searching in the direction of steepest descent $-(\gamma\vec{w} + \rho\nabla q)$, as an alternative to tackling the all-at-once system, and indeed descent methods are frequently considered for non-linear PDE-constrained problems. Examples of solving problems of the form (9) with two different strategies are presented in Section IV.

III. NUMERICAL METHODS

In order to solve the DDFT model (8) and control problem (9), appropriate numerical methods have to be used that are

accurate enough to resolve particle-scale information, while being efficient enough to solve the models in reasonable time. This difficulty is exacerbated by the non-local integral terms in the DDFT and control problems, complicated non-linear and non-local boundary conditions, as well as the solution of all of these on complicated domains. Moreover, the additional volume exclusion terms introduced into the DDFT model can become challenging as the packing fraction $\eta \to 1$, since the model becomes singular, and typical numerical methods become unstable. In the following subsections, the approaches for solving the DDFT model and control problem are discussed.

A. Pseudospectral and Spectral Element Methods

Pseudospectral methods are an established approach for solving DDFT problems, such as (8). An overview of pseudospectral methods can be found in [7] and [59]. 2DChebClass[21] is a computational framework in MATLAB, which enables users to solve model equations on simple domains in one and two dimensions using such pseudospectral approaches. We refer to [1] and [21] for a detailed discussion, and outline the key features below.

Chebyshev pseudospectral methods are based on polynomial interpolation through non-equispaced collocation points. This optimal distribution of collocation points avoids the Runge phenomenon (i.e., large oscillations on the boundary of the domain caused by interpolation on equispaced points), and therefore allows accurate approximations using high-order polynomials. This makes pseudospectral methods highly accurate when approximating smooth functions, and convergence is exponential for analytic functions[7]. The method produces small, dense matrices (when compared to large, sparse matrices typically obtained in finite difference and finite element methods, for example). Therefore, the method is not adversely affected when a problem contains non-local integral terms, such as convolutions, which will necessarily result in dense matrix systems irrespective of the chosen numerical method. Additionally, one can employ Clenshaw–Curtis quadrature[15] to approximate convolution integrals such as those arising in (8). This reduces the approximation of a convolution integral to a matrix–vector multiplication, in which the matrix can be precomputed and does not have to be formed at each iteration of a solver, for example, during timestepping in a PDE solver. An alternative approach is to use Fast Fourier Transform (FFT) methods, which require that the Fourier transform and inverse transform have to be taken at each iteration. Whilst the FFT approach is computationally cheaper for large numbers of grid points, comparing these two approaches directly is difficult: Pseudospectral methods typically use small numbers of points, and so the typical 'large-N' computational complexities may not be relevant; and the application of FFT to non-periodic domains, such as the complicated domains of interest in the present work, generally requires that the domains are 'padded' and then defined to be periodic, which both increases the number of computational points required, and also presents challenges in applying boundary conditions.

Relevant applications of the pseudospectral framework include the solution of different DDFT models[19,20], DFT problems[54,55], and other PDE applications[8,60]. The methods have also been extended to solving three-dimensional problems and optimal control problems[2]. Recently, in [41], the authors extended the pseudospectral framework to include a spectral element method (SEM). Spectral element methods utilize a pseudospectral grid on each geometric element and combine the elements to create the more complicated domain. There exist different SEM approaches, which can broadly be classed into Galerkin and patching methods. Galerkin SEM uses the weak form of the PDE model, while patching methods treat the strong form of the PDE directly, imposing matching conditions (patching) between individual elements. In the present work, the latter approach is applied, in line with the pre-existing framework for solving the strong form of PDEs on simple domains. A comprehensive introduction to spectral element methods can be found in [9] and [10].

With the SEM approach one can compute solutions to DDFT problems on complicated domains without losing the benefits from pseudospectral approaches. One numerical implementation is MultiShape, and as for the pseudospectral method, an open-source package is available[42]. The MultiShape package utilizes the pseudospectral 2DChebClass package for simple shapes, which allows precomputation of several quantities on individual geometric elements that make up a multishape[1]. The complicated domain, i.e., multishape, is constructed by combining these elements and imposing matching conditions at the intersection boundaries between them. The chosen matching conditions in the present work are continuity conditions, enforcing continuity of density and flux. An example of such a domain can be seen in Figure 4.

Both the 2DChebClass and MultiShape libraries are used in the present work to discretize DDFT models. A differential–algebraic equation (DAE) solver can then be applied to solve the discretized system, such as `ode15s` in MATLAB.

B. Newton–Krylov and Gradient Descent Approaches

For control problems such as (9), the resulting first-order optimality system accounts for the PDE constraint in (9), adjoint equation (10), and descent direction $\gamma \vec{w} + \rho \nabla q$. One may eliminate the resulting gradient equation by substituting it into the other two equations to obtain a coupled system of PDEs. The spatial discretization of this system is done as described above, using the 2DChebClass and MultiShape libraries. However, one is not able to apply standard DAE solvers since the PDE constraint has an initial condition and positive Laplacian structure, while the adjoint equation has a final-time condition and a negative Laplacian term. In order to tackle the *all-at-once* system with this forward–backward

---

[1] Note that 'MultiShape', with capital letters, refers to the software package, while a lower-case 'multishape' refers to a complex domain of interest.

structure in time, we apply a bespoke, robust solution strategy. In line with previous work, we utilize the Newton–Krylov algorithm[25], which minimizes a global-in-time residual vector. The method is accurate and computationally cheap due to the spectral-in-space-and-time discretization and efficient preconditioning. The Newton–Krylov method has been applied to mean-field DDFT optimal control problems on simple domains in [2] and on complicated domains in [41].

We also examine a variant of the gradient descent method of [58, Algorithm 4.1], tailored to the problem (9). As above, this is a potent and viable approach for reducing the value of the cost functional $\mathcal{J}(\rho, \vec{w})$ from that obtained from a solution of the state equation with no control applied, which is a key aim, and has been applied to a wide range of non-linear problems in the literature. This algorithm involves successively solving the state equation (9) for ρ given $\vec{w}$, solving the adjoint equation (10) for q given ρ and $\vec{w}$, moving the control in the direction of steepest descent multiplied by a mixing parameter scaled by γ, and a backtracking line-search to ensure a decrease in the estimate of the cost functional $\mathcal{J}(\rho, \vec{w})$ at each iteration. The forward and adjoint solves may be applied using the pseudospectral approach presented in this section, in the adjoint case by mapping to an initial value problem through a transformation of the time variable.

IV. NUMERICAL EXAMPLES

In this section, we present numerical examples for the DDFT model (8) and the corresponding control problem (9). In all examples $a = \pi/4$ (i.e., $\sigma = 1$) unless stated otherwise. The two-body interaction term is given by

$$V_2(\|\vec{x}\|) = \kappa e^{-\|\vec{x}\|^r/\sigma}, \tag{11}$$

where κ and r are specified in the text below; in particular, we choose $r = 1$ or $r = 2$, and κ will always be negative, modelling an attractive, long-range interaction or zero, when we neglect mean-field interactions. Note that the results are robust under changes to the interaction potential, external forcing, domain and initial conditions. All tests are computed on Dell PowerEdge R430 running Scientific Linux 7, four Intel Xeon E5-2680 v3 2.5GHz cores, 30M Cache, 9.6 GT/s QPI 192 GB RAM, using MATLAB Version 2022b.

A. Solving DDFT Models

In this section problem (8) is solved. The DDFT model is investigated by comparing it to the mean-field DDFT model (i.e., by removing the volume exclusion term j_{VE}). Then, the effect of choosing two different kinds of boundary conditions is discussed, by comparing the effect of no-flux and periodic boundary conditions. Finally, a DDFT model is solved on a multishape domain, for two different sizes of particles. For all examples the DAE solver $\texttt{ode15s}$[52,53] in MATLAB is used. The solver's relative and absolute tolerances are set to 10^{-7}, unless stated otherwise.

1. Comparison with a Previous Model

In this paper, we have added the term j_{VE} to the mean-field DDFT model to capture volume exclusion effects. This means that particles cannot overlap and therefore we expect that they cannot be packed as densely as in the mean-field model without the term j_{VE}. We choose weakly attractive particles that experience a gravitational force given by the potential $V_{ext} = 0.1x_2$. The interactions are defined by the potential (11), with $r = 2$ and $\kappa = -0.5$. The temporal–spatial domain is $(0, 10) \times [0, 20] \times [0, 15]$, with $N_1 = N_2 = 20$ spatial discretization points. The initial condition for ρ is given by

$$\rho(0, \vec{x}) = \bar{\rho},$$

where $\bar{\rho}$ is a constant, denoting the average particle density. Each example takes around half a second to solve.

We compare the solution of the model (8) without the volume exclusion term j_{VE} with the model that includes j_{VE}, for varying $\bar{\rho}$. In Figure 1, this is presented at time $t = 10$ for $\bar{\rho} = 0.1, 0.3, 0.5$ (i.e., 30, 90, 150 particles, respectively). It is evident that in all cases the model with volume exclusion permits less particle clustering than the model without j_{VE}, as expected. For lower densities, the two models exhibit similar results, while for higher densities, the two different models produce very different results. This demonstrates that volume exclusion can be an important feature when modelling particle dynamics, such as sedimentation phenomena, as discussed above.

2. The Choice of Boundary Conditions

In [5], it was investigated how attractive particles impact sedimentation processes, using model (8) with periodic boundary conditions. The authors chose a temporal–spatial domain $(0, 300) \times [0, 64] \times [0, 43.5]$. The particles experience the effect of an external gravitational potential given by $V_{ext} = 0.1x_2$ and particle–particle interactions given by the potential (11), where $r = 1$, $\sigma = 1$, and $\kappa = -3.5$.

Two DDFT solutions are presented in [5], both computed in a periodic box, with the left and right boundaries being periodic and the top and bottom boundaries modelled as hard walls, using an infinite external potential for $x_2 < 0$ and $x_2 > 43.5$. The first result is computed with an average density $\bar{\rho} = 0.072$ (i.e., 188 particles), while the second model has average density $\bar{\rho} = 0.2$ (i.e., 522 particles). The initial condition is given by

$$\rho(0, \vec{x}) = \bar{\rho} \pm \frac{\xi(\vec{x})}{20}\bar{\rho},$$

where $\xi(\vec{x})$ is a random field generated (numerically) by sampling from a uniform random variable in $[0, 1]$ at each discretization point. Note that $\bar{\rho}$ constitutes a steady state for a system with periodic boundary conditions and no advection, and the perturbation is added to induce dynamics. However, for a system with no-flux boundary conditions (such as the
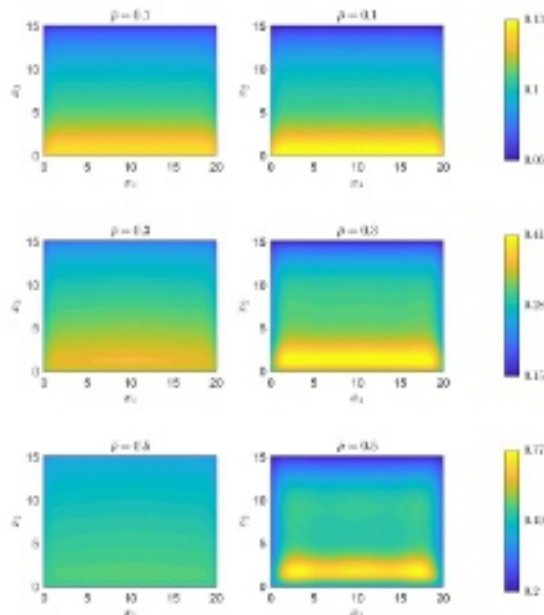
FIG. 1: Comparison of a model problem with volume exclusion term j_{VE} present (left) and without volume exclusion (right) for different average particle densities $\bar{\rho}$ at $t = 10$.

one presented below) this perturbation is technically not required, since $\bar{\rho}$ is not a steady state. For both choices of $\bar{\rho}$, phase separation occurs and the particles form a small number of clusters. The authors in [5] find that for lower densities, at later times, the particles form a finite number of clusters on the bottom of the domain, while for the higher density example the particles form a single layer of particles. This is explained by the fact that the particle density minimizes the free energy in the system, which in the lower density regime causes the individual clusters.

Here, we replicate the results with one important adjustment, namely that the hard walls are not imposed by an external potential but the no-flux boundary conditions are applied directly. We choose $N_1 = N_2 = 100$ computational points, since the phase separation is challenging to resolve numerically. The computational time for the problem with $\bar{\rho} = 0.072$ is around 3 hours, while the time to compute the problem with $\bar{\rho} = 0.2$ is around 11 hours. This demonstrates the increased difficulty of the problem with increased mass in the system. Figures 2a and 3a show the resulting density profiles at different times. These are similar to those reported in [5], and the predicted clustering for $\bar{\rho} = 0.072$, as well as the uniform density layer for $\bar{\rho} = 0.2$ at later times is found. There is a difference in the density evolution for the model with $\bar{\rho} = 0.2$ when compared to the result in [5]. In [5], individual clusters form throughout the domain before the density layer forms at later times. In our simulation, several density layers form, before the characteristic single density layer is created. These differ-

ences may be caused by the different initial noise, or by the application of no-flux conditions at the top and bottom walls, instead of the use of a confining external potential modelling hard walls.

Next, the same experiments are carried out but with no-flux conditions on all four boundaries; see Figures 2b and 3b. The computational times here are around 12 hours for the problem with $\bar{\rho} = 0.072$ and around 16 hours for the problem with $\bar{\rho} = 0.2$. This demonstrates that the problem with no-flux boundary conditions is more challenging to solve numerically than the problem with periodic conditions. Comparing the results in Figure 2a and 2b, it is evident that although the particles form a number of clusters in both cases, they do exhibit differences. Since the periodic problem does not have a boundary in x_1, initially the particles only arrange in lines, before the particle clusters arrange in an approximately evenly-spaced manner in x_1. In the example with no-flux boundary conditions, there is now a boundary in the x_1 direction and particles cluster earlier in the simulation and closer to the middle of the domain. Therefore, at later times, the middle cluster is larger than the other clusters of particles. A similar effect can be observed for the simulation with $\bar{\rho} = 0.2$ displayed in Figure 3b. The particles form clusters, rather than lines, due to the symmetry breaking in x_1 caused by the no-flux boundary conditions. Over time, differently sized, larger clusters form, before one uniform cluster of particles is created at later times. This resembles the single particle layer found for the periodic domain, but the no-flux condition prevents the spread of particles to the walls at $x_1 = 0$ and $x_1 = 64$. These effects are caused by the fact that the particles attract each other. In the domain with no-flux conditions, a larger number of particles come into contact with each other in the middle of the domain than on the boundaries, and hence more clusters form in the centre of the domain. Equivalently, the free energy is lowered with a higher density in the middle of the domain than at the boundaries.

3. Solving the DDFT Model on a Multishape

We consider a multishape consisting of three elements; see Figure 4. Each element contains $N_1 = N_2 = 20$ points in each spatial direction. We choose 10^{-9} as absolute and relative tolerances in the DAE solver. The following example models a silo through which particles are passing. The set-up is motivated by examples of particle dynamics in silos under gravity[6]. However, problems such as yeast sedimentation in brewing vessels[62], wastewater treatment in sedimentation tanks[23], and pharmaceutical production in centrifuges[30] can also be modelled using this set-up.

We consider two examples: in the first, the particles are smaller, in the second they are larger, so that different qualitative behaviour is expected in each case. In the first example, an external potential is imposed, modelling gravitational forces, as well as repulsive effects with the silo walls. It is defined by $V_{ext}(\vec{x}) = 0.15x_2 + \varepsilon \left(\exp\left(-(d_L(\vec{x})/\alpha)^2\right) + \exp\left(-(d_R(\vec{x})/\alpha)^2\right) \right)$. The parameters are set to $\varepsilon = 0.6$, $\alpha = 0.5$, and, at each point $\vec{x}$ in the

(a) Periodic boundary conditions
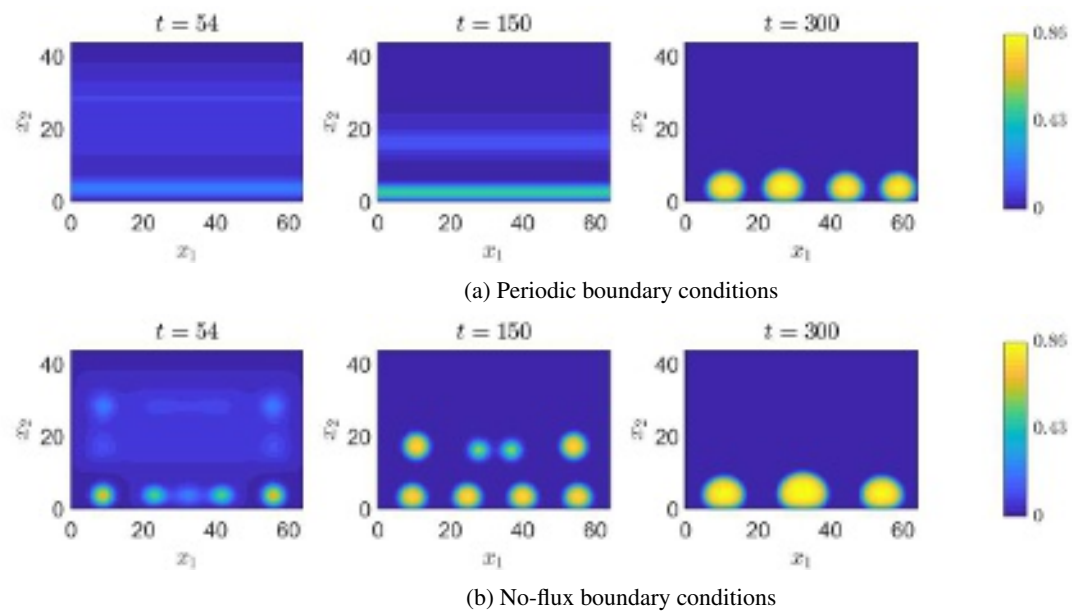

(b) No-flux boundary conditions

FIG. 2: Sedimentation of attractive particles in a box with (a) periodic and (b) no-flux boundary conditions, with an average density of $\bar{\rho} = 0.072$.
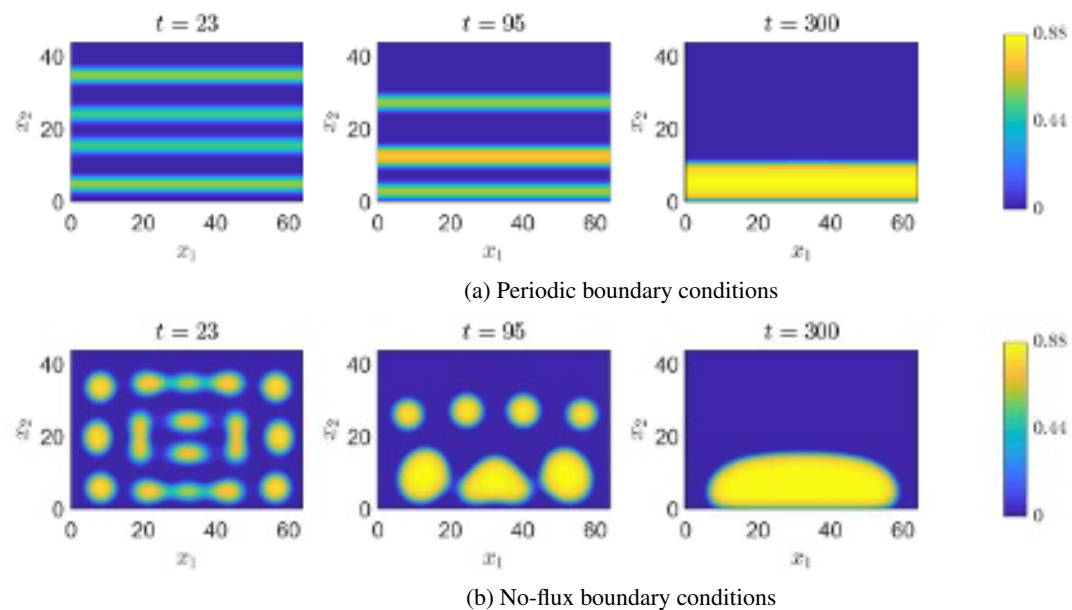

(a) Periodic boundary conditions

(b) No-flux boundary conditions

FIG. 3: Sedimentation of attractive particles in a box with (a) periodic and (b) no-flux boundary conditions, with an average density of $\bar{\rho} = 0.2$.

domain, d_L, d_R are the shortest (Euclidean) distances to the left and right walls of the silo, respectively. The interaction potential for this example is given by (11), with $r = 2$, $\sigma = 0.5$, and $\kappa = -0.1$. The initial conditions are

$$\rho(0, \vec{x}) = \frac{20 f_{\text{ic}}}{\int_\Omega f_{\text{ic}} d\vec{x}}, \text{ with } f_{\text{ic}} = x_2 + 5.$$

The time interval for this simulation is $t \in [0, 20]$. The setup for the second example is identical, but with $\alpha = \sigma = 2$.

The solution of each example takes around 50 seconds, and the solutions can be seen in Figure 5. One can observe that in each example the particles are affected by gravity, are repulsed from the left and right walls, and cluster due to attractive interaction forces. The key difference between the two examples is due to the sizes in particles. In Figure 5a, one can observe that the particles are able to accumulate closer to the silo walls than those in Figure 5b, since they are smaller. Moreover, more particles are able to pass through the narrow
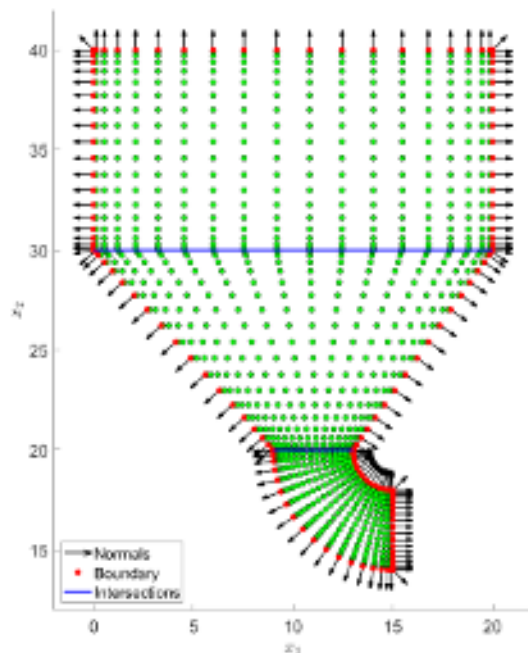
FIG. 4: A multishape with three elements.

part of the silo at the bottom. In the second example particles accumulate above the narrow tube since they are larger and therefore cannot easily pass through due to volume exclusion.

B. Solving Control Problems

We are now in the position to consider control problems of the form (9). In particular, we wish to provide a proof-of-concept that our pseudospectral and MultiShape approaches can be applied within all-at-once or gradient descent solvers for such problems. We first compare the model with volume exclusion term j_{VE} present and absent, as done for the DDFT model, before presenting a control problem on a multishape using the full volume-excluding model. The system is described by the PDE constraint in (9), the adjoint equation (10), and the descent direction. For each problem the performance of our algorithm is tested by evaluating the cost functional $\mathscr{J}$ before optimization (i.e., when $\vec{w} = \vec{0}$) and after optimization (using the Newton–Krylov method). The respective values are denoted by $\mathscr{J}_{uc}$ and $\mathscr{J}_c$. We note again the possibility of encountering local optima, due to the non-linearity of the problem considered, as opposed to global minima, so the measure of performance we look for is a reduction of $\mathscr{J}$. One is required to provide an initial guess for the solver, which is given by $\rho(t,\vec{x}) = \rho(0,\vec{x})$ and $q(t,\vec{x}) = q(T,\vec{x}) = 0$ for all t. Additional inputs for the Newton–Krylov algorithm are the tolerance 10^{-16}, a maximum of 10 Newton iterations, and a maximum of 200 GMRES iterations. For the descent algorithm of the form devised in [58] we set a tolerance (to measure the convergence of the control) of 10^{-5}, an initial mixing parameter of 0.8, and a minimum allowable mixing parameter of 10^{-5}.

1. Comparison Between the Two Models

As for the DDFT model, we would like to investigate the effect of the additional term j_{VE} on the model, and consequently on a corresponding control problem. For this, we consider the example presented in Section IV A 1 with $\bar{\rho} = 0.4$ (i.e., 120 particles) and interaction strength $\kappa = -0.3$. The desired state $\widehat{\rho}$ is given by the solution to the DDFT model (8) with volume exclusion term j_{VE} included and $V_{ext} = 0.1x_2$. The control problems are solved numerically with $V_{ext} = 0$, so we expect the control to act as a gravitational force to drive ρ towards $\widehat{\rho}$. We choose a time horizon $(0, 10)$, and spatial domain $[0,20] \times [0,15]$, with $N_1 = N_2 = 20$ discretization points in space, and $n = 11$ points in time. We note that the Newton–Krylov results presented here are robust upon increasing the number of discretization points.

Solving the control problem using the Newton–Krylov solver, with γ in the range 10^{-4} to 10^{-2}, takes around 5–10 minutes. Note that the method works for a significantly wider range of γ but we restrict the range here to allow a comparison with the descent method[58], within which the PDE solver used demonstrated robustness for a smaller range of γ. In Table I we present the cost for the uncontrolled ($\mathscr{J}_{uc}$) and controlled problems ($\mathscr{J}_c$) both with (top) and without (bottom) volume exclusion. Note the significant reduction of the cost functional under imposition of non-zero control.

In Figure 6, the solutions for both models with $\gamma = 10^{-3}$ are presented. It is evident that while the particle distributions are similar with and without volume exclusion, due to the choice of γ, the controls for the two models act in different ways. While the control for the model including j_{VE} acts downwards, in lieu of the gravitational force, the control of the model without volume exclusion invests more control to spread the particles out, since in this model the particles are allowed to cluster more tightly than in the target state, created with the volume-excluding model.

One validation of our results was obtained by inserting the control from our Newton–Krylov method into the descent algorithm[58]. In all cases presented, the resulting control differs by less than 2%, measured in a relative L^2 norm in time and space. The descent algorithm typically takes around 1 minute to run, primarily a consequence of the extremely efficient pseudospectral solver. We also found that the descent algorithm converges to these solutions when the initial guess is perturbed somewhat away from the result from the Newton–Krylov scheme. However, as discussed, since the problem is non-linear, there is a possibility of encountering local minima. For example, we found that starting with an initial guess of zero control for the descent algorithm in the case $\gamma = 10^{-2}$ with volume exclusion resulted in a control with cost 9.08×10^{-2}, which is slightly better than that found by our Newton–Krylov approach. In contrast, for $\gamma = 10^{-3}$ the cost resulting from an initial guess of zero control was larger than

Accepted to J. Chem. Phys. 10.1063/5.0166458

DDFT for Sedimentation Processes

10

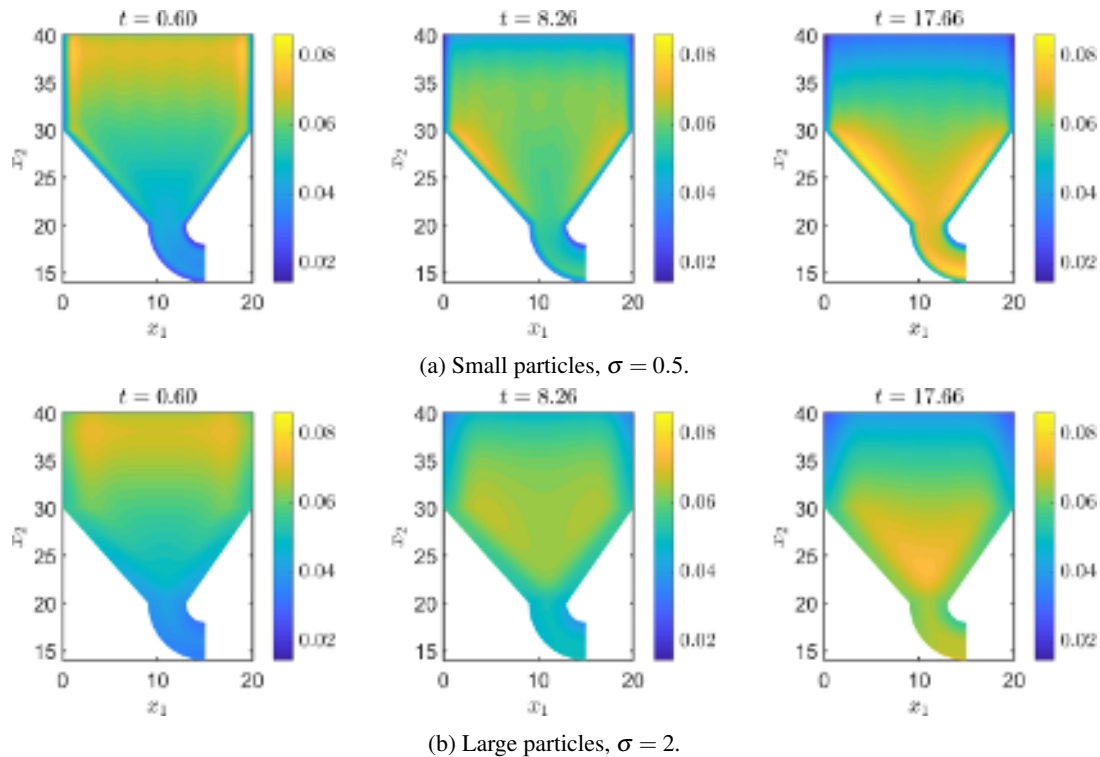(a) Small particles, $\sigma = 0.5$.

(b) Large particles, $\sigma = 2$.

FIG. 5: Two examples of particle dynamics under gravity with volume exclusion: (a) smaller particles with $\sigma = 0.5$, (b) larger particles with $\sigma = 2$.

	$\gamma = 10^{-4}$	$\gamma = 10^{-3}$	$\gamma = 10^{-2}$
$\mathscr{J}_{uc}$	1.03	1.03	1.03
$\mathscr{J}_c$	1.55×10^{-3}	1.42×10^{-2}	1.15×10^{-1}
$\mathscr{J}_{uc}$	1.29	1.29	1.29
$\mathscr{J}_c$	4.36×10^{-3}	1.19×10^{-2}	7.87×10^{-2}

TABLE I: Values of the cost functional $\mathscr{J}$ for a control problem, computed on a box with no-flux boundary conditions with (top) and without (bottom) volume exclusion. The value of the cost functional of the uncontrolled problem with $\vec{w} = \vec{0}$, denoted by $\mathscr{J}_{uc}$, is compared to the cost of the controlled problem $\mathscr{J}_c$ for different values of γ.

that found with the Newton–Krylov method. Additionally, the descent algorithm failed to converge for the zero initial guess (due to failure of the PDE solver under large perturbations of the control) for $\gamma = 10^{-4}$ and $\gamma = 10^{-1}$; we believe this issue could be circumvented by using more discretization points in the PDE solver, or a bespoke choice of the mixing parameter, but this would significantly increase the computational time of the descent algorithm and require problem-dependent insight. We highlight that our Newton–Krylov scheme does succeed in reducing the cost functional for this problem, under a wide range of initial guesses of the density and adjoint, as well as choices of discretization.

Note that we do not choose a $\widehat{\rho}$ created from a DDFT model without volume exclusion. The reason for this is that, for the
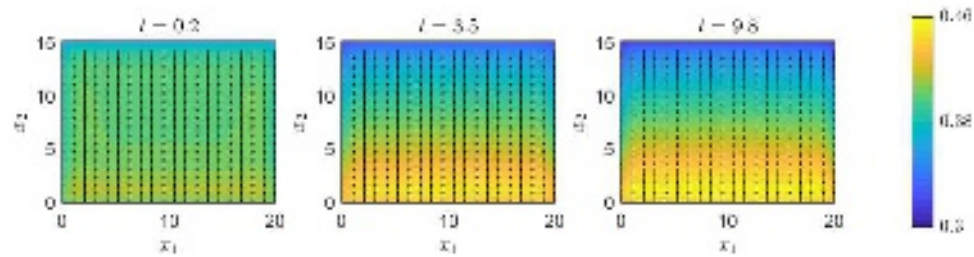
problem with the term j_{VE} present, the control variable would attempt to push the particles to cluster more tightly than the volume exclusion property of this model allows. This would cause numerical issues, since $\rho \to 1/a$ (i.e., $\eta \to 1$) in this case, causing the term j_{VE} to become very large and numerically unstable.

2. An Example using MultiShape

We now solve the control problem (9) numerically on a MultiShape domain, consisting of one quadrilateral and one wedge element, using the Newton–Krylov scheme. The time horizon is $(0, 2)$. Each element is discretized by $N_1 = N_2 = 20$ collocation points, and $n = 11$. The initial condition for ρ is

$$\rho(0, \vec{x}) = Z^{-1} \exp(-0.5(x_1 - 0.75)^2 - 0.5(x_2 - 3.3)^2),$$

where Z is a normalization constant, which results in an average density of $\bar{\rho} = 0.1$. The particles in this problem do not experience any particle–particle interactions (i.e., $\kappa = 0$), and no external potential. However, the desired state $\widehat{\rho}$ is designed by computing the model problem (8), including interaction potential (11), with $r = 2$ and $\kappa = -1$, as well as external potential $V_{ext} = 0.5x_2$. Therefore, we expect the control $\vec{w}$ to simulate attractive particle–particle and gravitational forces. Computing the solution for $\gamma = 10^{-3}$ takes around 30 minutes and the result is displayed in Figure 7. It is evident that the control forces the particles together and down the channel, as

Accepted to J. Chem. Phys. 10.1063/5.0166458

DDFT for Sedimentation Processes   11

(a) Control problem (9), with volume exclusion term j_{VE} present.
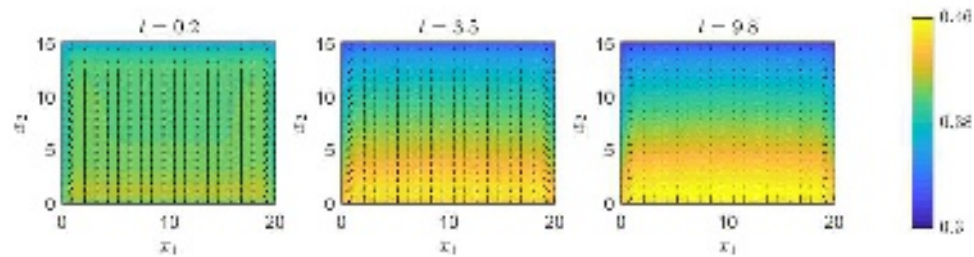
(b) Control problem (9), without volume exclusion.

FIG. 6: Comparison between the solution ρ and control $\vec{w}$ for $\gamma = 10^{-3}$ with the volume exclusion term j_{VE} (a) included and (b) excluded. Shown are computed density ρ (colour) and superimposed control $\vec{w}$ (arrows).

expected. In Table II, the resulting values of the cost functional for different choices of γ are compared to those of the uncontrolled problem. As expected, these become closer as the penalty for applying the control (γ) is increased.

	$\gamma = 10^{-5}$	$\gamma = 10^{-3}$	$\gamma = 10^{-1}$
$\mathscr{J}_{uc}$	2.07×10^{-4}	2.07×10^{-4}	2.07×10^{-4}
$\mathscr{J}_c$	3.13×10^{-6}	8.99×10^{-5}	2.05×10^{-4}

TABLE II: Values of the cost functional $\mathscr{J}$ for a control problem, computed on a multishape with no-flux boundary conditions and volume exclusion. The value of the cost functional of the uncontrolled problem with $\vec{w} = \vec{0}$, denoted by $\mathscr{J}_{uc}$, is compared to the cost of the controlled problem $\mathscr{J}_c$ for different values of γ.

V. SUMMARY

The resolution of sedimentation processes using the DDFT methodology is a problem of keen interest. Motivated by this, the present work illustrates that extensions of the DDFT model can be tackled with the method developed in [2, 41]. It was demonstrated that the framework is able to solve DDFT models with additional terms that describe volume exclusion, as well as corresponding control problems. The qualitative differences in solutions of models with and without volume exclusion were investigated, to demonstrate the importance of including such effects to accurately describe real-world hard particle systems. Moreover, the effect of different boundary

conditions was studied, comparing periodic and no-flux conditions, demonstrating that the results in modelling sedimentation and clustering dynamics are severely impacted by the choice of boundary conditions imposed.

A key motivation was to model hard particle dynamics on complicated domains that naturally arise in real-world applications. Since boundary conditions and volume exclusion demonstrably affect the dynamics, the ability to accurately apply the correct conditions needs to be included in the chosen methodology, which has been done successfully in the present work. Moreover, the present work not only addresses the question of how to simulate such processes, but also provides a framework for the control of hard particle dynamics on complicated domains, including no-flux boundary conditions. Production set-up in a range of applications, such as brewing, wastewater treatment, or processes in the pharmaceutical industry, can potentially be optimized using this framework.

It is evident that this extended model is numerically more challenging to solve than the mean-field DDFT, due to the terms that prescribe the volume exclusion. In order to solve a model of this form, more care has to be taken in ensuring that ρ does not become too large, i.e., that the packing fraction η does not approach unity, in any part of the domain at any time, and in particular that $0 < \rho < 1/a$. This extended DDFT model furthermore raises new theoretical questions about existence, uniqueness, and regularity of solutions, due to the form of the term j_{VE}. Since j_{VE} becomes unbounded as $\rho \to 1/a$, such questions require careful examination in future work.

The solution of a corresponding control problem posed additional challenges that had to be addressed. First, the deriva-
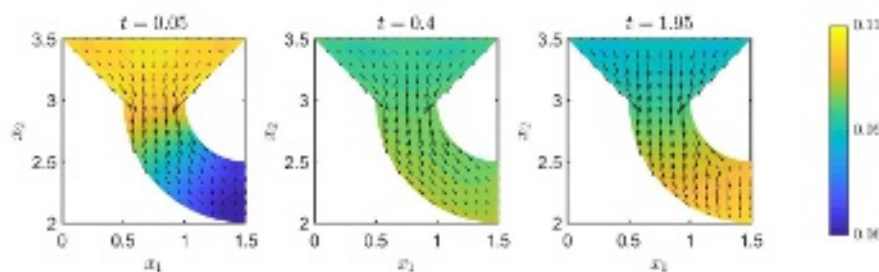
Accepted to J. Chem. Phys. 10.1063/5.0166458

DDFT for Sedimentation Processes   12

FIG. 7: The computed density ρ (colour) with superimposed control $\vec{w}$ (arrows) for a problem with volume exclusion effects.

tion of the first-order optimality system was more involved than that for the mean-field DDFT. The successful numerical solution of the control problem involving this extended model depended on both the choice $\widehat{\rho}$ and the corresponding ρ. While this is the case for many optimal control problems, for the present model the state ρ is required to satisfy $0 < \rho < 1/a$ for all $(t, \vec{x}) \in (0, T) \times \Omega$. Moreover, the choice of $\widehat{\rho}$ should likely also satisfy these bounds, since otherwise the control may act to push ρ outside its prescribed bounds towards $\widehat{\rho}$. In order to ensure these conditions on ρ are met, one could extend this methodology to include state or control constraints in future work.

Notwithstanding these open questions, the present implementation enables the modelling of volume exclusion effects on complicated domains that are important for capturing many real-world processes accurately. It furthermore demonstrates that the method introduced in [2,41] is, in principle, applicable to some of the more complicated extensions of DDFT, such as those discussed in [56].

DATA AVAILABILITY

The code required to reproduce the results of this work is available at https://bitbucket.org/bdgoddard/multishapesedimentation/src/.

ACKNOWLEDGEMENTS

[1] M. Aduamoah, B. D. Goddard, J. W. Pearson, and J. C. Roden. 2DChebClassPDECO [Software]. https://bitbucket.org/bdgoddard/2dchebclasspdecopublic/, 2020.

[2] M. Aduamoah, B. D. Goddard, J. W. Pearson, and J. C. Roden. Pseudospectral methods and iterative solvers for optimization problems from multiscale particle dynamics. *BIT Numerical Mathematics*, 62:1703–1743, 2022.

[3] G. Albi, Y.-P. Choi, M. Fornasier, and D. Kalise. Mean field control hierarchy. *Applied Mathematics & Optimization*, 76:93–135, 2017.

[4] A. J. Archer. Two-dimensional fluid with competing interactions exhibiting microphase separation: Theory for bulk and interfacial properties. *Physical Review E*, 78(3):031402, 2008.

[5] A. J. Archer and A. Malijevský. On the interplay between sedimentation and phase separation phenomena in two-dimensional colloidal fluids. *Molecular Physics*, 109(7–10):1087–1099, 2011.

[6] D. Bertuola, S. Volpato, P. Canu, and A. C. Santomaso. Prediction of segregation in funnel and mass flow discharge. *Chemical Engineering Science*, 150:16–25, 2016.

[7] J. P. Boyd. *Chebyshev and Fourier Spectral Methods*. Dover Publications, Inc., Mineola, New York, 2nd edition, 2000.

[8] P. Buttà, B. Goddard, T. M. Hodgson, M. Ottobre, and K. J. Painter. Non-mean-field Vicsek-type models for collective behaviour. *Mathematical Models and Methods in Applied Sciences*, 32(14):2763–2816, 2022.

[9] C. Canuto, M. Y. Hussaini, A. Quarteroni, and T. A. Zang. *Spectral Methods in Fluid Dynamics*. Springer Berlin, Heidelberg, 1988.

[10] C. Canuto, A. Quarteroni, M. Y. Hussaini, and T. A. Zang. *Spectral Methods: Evolution to Complex Geometries and Applications to Fluid Dynamics*. Springer Berlin, Heidelberg, 2007.

[11] E. Casas and V. Dhamo. Error estimates for the numerical approximation of Neumann control problems governed by a class of quasilinear elliptic equations. *Computational Optimization and Applications*, 52(3):719–756, 2012.

[12] C. Chalmers, R. Smith, and A. J. Archer. Dynamical density functional theory for the evaporation of droplets of nanoparticle suspension. *Langmuir*, 33(50):14490–14501, 2017.

[13] A. Chamoux and A. Perera. Approximations for the direct correlation function in multicomponent molecular fluids. *The Journal of Chemical Physics*, 104(4):1493–1505, 1996.

[14] A. Chamoux and A. Perera. Direct correlation functions in two-dimensional anisotropic fluids. *Physical Review E*, 58(2):1933–1947, 1998.

[15] C. W. Clenshaw and A. R. Curtis. A method for numerical integration on an automatic computer. *Numerische Mathematik*, 2:197–205, 1960.

[16] J. A. de la Torre, P. Español, and A. Donev. Finite element discretization of non-linear diffusion equations with thermal fluctuations. *The Journal of Chemical Physics*, 142(9):094115, 2015.

[17] S. DuBois and A. Perera. Entropy driven demixing in fluids of rigidly ordered particles. *The Journal of Chemical Physics*, 116(14):6354–6367, 2002.

[18] R. Evans. The nature of the liquid-vapour interface and other topics in the statistical mechanics of non-uniform, classical fluids. *Advances in Physics*, 28(2):143–200, 1979.

[19]B. D. Goddard, T. D. Hurst, and R. Ocone. Modelling inelastic granular media using dynamical density functional theory. *Journal of Statistical Physics*, 183:Art. 6, 2021.

[20]B. D. Goddard, A. Nold, and S. Kalliadasis. Dynamical density functional theory with hydrodynamic interactions in confined geometries. *The Journal of Chemical Physics*, 145(21):214106, 2016.

[21]B. D. Goddard, A. Nold, and S. Kalliadasis. 2DChebClass [Software]. `http://dx.doi.org/10.7488/ds/1991`, 2017.

[22]A. González, J. A. White, and R. Evans. Density functional theory for hard-sphere fluids: a generating function approach. *Journal of Physics: Condensed Matter*, 9(11):2375–2398, 1997.

[23]A. M. Goula, M. Kostoglou, T. D. Karapantsios, and A. I. Zouboulis. The effect of influent temperature variations in a sedimentation tank for potable water treatment—A computational fluid dynamics study. *Water Research*, 42(13):3405–3414, 2008.

[24]H. Graf and H. Löwen. Phase diagram of tobacco mosaic virus solutions. *Physical Review E*, 59(2):1932–1942, 1999.

[25]S. Güttel and J. W. Pearson. A spectral-in-time Newton–Krylov method for nonlinear PDE-constrained optimization. *IMA Journal of Numerical Analysis*, 42(2):1478–1499, 2022.

[26]J.-P. Hansen. *Theory of Simple Liquids: With Applications to Soft Matter*. Academic Press, Amsterdam, 4th edition, 2013.

[27]D. Helbing. Traffic and related self-driven many-particle systems. *Reviews of Modern Physics*, 73(4):1067–1141, 2001.

[28]D. Helbing, L. Buzna, A. Johansson, and T. Werner. Self-organized pedestrian crowd dynamics: Experiments, simulations, and design solutions. *Transportation Science*, 39(1):1–24, 2005.

[29]E. Helfand, H. L. Frisch, and J. L. Lebowitz. Theory of the two- and one-dimensional rigid sphere fluids. *The Journal of Chemical Physics*, 34(3):1037–1042, 1961.

[30]S. O. Majekodunmi. A review on centrifugation in the pharmaceutical industry. *American Journal of Biomedical Engineering*, 5(2):67–78, 2015.

[31]A. Malijevský and A. J. Archer. Sedimentation of a two-dimensional colloidal mixture exhibiting liquid-liquid and gas-liquid phase separation: a dynamical density functional theory study. *The Journal of Chemical Physics*, 139(14):144901, 2013.

[32]Y. Martínez-Ratón, J. A. Capitán, and J. A. Cuesta. Fundamental-measure density functional for mixtures of parallel hard cylinders. *Physical Review E*, 77(5):051205, 2008.

[33]Á. Mulero. *Theory and Simulation of Hard-Sphere Fluids and Related Systems*. Springer Berlin, Heidelberg, 2008.

[34]R. K. Pathria and P. D. Beale. *Statistical Mechanics*. Academic Press, Amsterdam, 4th edition, 2021.

[35]J. K. Percus. Equilibrium state of a classical fluid of hard rods in an external field. *Journal of Statistical Physics*, 15(6):505–511, 1976.

[36]J. K. Percus and G. J. Yevick. Analysis of classical statistical mechanics by means of collective coordinates. *Physical Review*, 110(1):1–13, 1958.

[37]T. V. Ramakrishnan and M. Yussouff. First-principles order-parameter theory of freezing. *Physical Review B*, 19(5):2775–2794, 1979.

[38]A. Ravindran, P. Chandran, and S. S. Khan. Biofunctionalized silver nanoparticles: advances and prospects. *Colloids and Surfaces B: Biointerfaces*, 105:342–352, 2013.

[39]H. Reiss, H. L. Frisch, E. Helfand, and J. L. Lebowitz. Aspects of the statistical thermodynamics of real fluids. *The Journal of Chemical Physics*, 32(1):119–124, 1960.

[40]H. Reiss, H. L. Frisch, and J. L. Lebowitz. Statistical mechanics of rigid spheres. *The Journal of Chemical Physics*, 31(2):369–380, 1959.

[41]J. C. Roden, R. D. Mills-Williams, J. W. Pearson, and B. D. Goddard. MultiShape: A spectral element method, with applications to Dynamic Density Functional Theory and PDE-constrained optimization. *arXiv preprint arXiv:2207.05589*, 2022.

[42]J. C. Roden, R. D. Mills-Williams, J. W. Pearson, and B. D. Goddard. MultiShape [Software]. `https://bitbucket.org/bdgoddard/multishapepublic/src/master/`, 2022.

[43]Y. Rosenfeld. Scaled field particle theory of the structure and the thermodynamics of isotropic hard particle fluids. *The Journal of Chemical Physics*, 89(7):4272–4287, 1988.

[44]Y. Rosenfeld. Free-energy model for the inhomogeneous hard-sphere fluid mixture and density-functional theory of freezing. *Physical Review Letters*, 63(9):980–983, 1989.

[45]Y. Rosenfeld. Free-energy model for the inhomogeneous hard-sphere fluid in D dimensions: Structure factors for the hard-disk ($D = 2$) mixtures in simple explicit form. *Physical Review A*, 42(10):5978–5989, 1990.

[46]R. Roth. Fundamental measure theory for hard-sphere mixtures: a review. *Journal of Physics: Condensed Matter*, 22(6):063102, 2010.

[47]R. Roth. Fluid of discs with competing interactions. *Molecular Physics*, 109(23–24):2897–2905, 2011.

[48]R. Roth, K. Mecke, and M. Oettel. Communication: Fundamental measure theory for hard disks: Fluid and solid. *The Journal of Chemical Physics*, 136(8):081101, 2012.

[49]A. Russo, S. P. Perez, M. A. Durán-Olivencia, P. Yatsyshin, J. A. Carrillo, and S. Kalliadasis. A finite-volume method for fluctuating dynamical density functional theory. *Journal of Computational Physics*, 428:109796, 2021.

[50]M. Schmidt, H. Löwen, J. M. Brader, and R. Evans. Density functional theory for a model colloid–polymer mixture: bulk fluid phases. *Journal of Physics: Condensed Matter*, 14(40):9353–9382, 2002.

[51]F. Schwabl. *Statistical Mechanics*. Springer Berlin, Heidelberg, 2nd edition, 2006.

[52]L. F. Shampine and M. W. Reichelt. The MATLAB ODE suite. *SIAM Journal on Scientific Computing*, 18(1):1–22, 1997.

[53]L. F. Shampine, M. W. Reichelt, and J. A. Kierzenka. Solving index-1 DAEs in MATLAB and Simulink. *SIAM Review*, 41(3):538–552, 1999.

[54]Y. Sun, Z. Dai, G. Shen, X. Lu, X. Ling, and X. Ji. Accelerate the electrolyte perturbed-chain statistical associating fluid theory–Density Functional Theory calculation with the Chebyshev pseudo-spectral collocation method. Part II. spherical geometry and Anderson mixing. *Frontiers in Chemistry*, 9:801551, 2021.

[55]Y. Sun, X. Lu, G. Shen, and X. Ji. Accelerate the ePC-SAFT-DFT calculation with the Chebyshev pseudospectral collocation method. *Industrial & Engineering Chemistry Research*, 60(25):9269–9285, 2021.

[56]M. te Vrugt, H. Löwen, and R. Wittkowski. Classical dynamical density functional theory: from fundamentals to applications. *Advances in Physics*, 69(2):121–247, 2020.

[57]A. L. Thorneywork, S. K. Schnyder, D. G. A. L. Aarts, J. Horbach, R. Roth, and R. P. A. Dullens. Structure factors in a two-dimensional binary colloidal hard sphere system. *Molecular Physics*, 116(21–22):3245–3257, 2018.

[58]R. J. Tomlin, S. N. Gomes, G. A. Pavliotis, and D. T. Papageorgiou. Optimal control of thin liquid films and transverse mode effects. *SIAM Journal on Applied Dynamical Systems*, 18(1):117–149, 2019.

[59]L. N. Trefethen. *Spectral Methods in MATLAB*. SIAM, Philadelphia, 2000.

[60]Z. Trstanova, B. Leimkuhler, and T. Lelièvre. Local and global perspectives on diffusion maps in the analysis of molecular systems. *Proceedings of the Royal Society A*, 476(2233):20190036, 2020.

[61]F. Tröltzsch. *Optimal Control of Partial Differential Equations: Theory, Methods and Applications*. American Mathematical Society, Providence, 2010.

[62]V. Vidgren and J. Londesborough. 125th anniversary review: Yeast flocculation and sedimentation in brewing. *Journal of the Institute of Brewing*, 117(4):475–487, 2011.

[63]J. Winkelmann. The liquid-vapour interface of pure fluids and mixtures: application of computer simulation and density functional theory. *Journal of Physics: Condensed Matter*, 13(21):4739–4768, 2001.

[64]O. Zvyagolskaya, A. J. Archer, and C. Bechinger. Criticality and phase separation in a two-dimensional binary colloidal fluid induced by the solvent critical behavior. *Europhysics Letters*, 96(2):28005, 2011.